

# Towards Robust Autonomous Grasping with Reflexes Using High-Bandwidth Sensing and Actuation

Andrew SaLoutos<sup>1</sup>, Hongmin Kim<sup>1</sup>, Elijah Stanger-Jones<sup>1</sup>, Menglong Guo<sup>1</sup>, and Sangbae Kim<sup>1</sup>

*Abstract*—Modern robotic manipulation systems fall short of human manipulation skills partly because they rely on closing feedback loops exclusively around vision data, which reduces system bandwidth and speed. By developing autonomous grasping reflexes that rely on high-bandwidth force, contact, and proximity data, the overall system speed and robustness can be increased while reducing reliance on vision data. We are developing a new system built around a low-inertia, high-speed arm with nimble fingers that combines a high-level trajectory planner operating at less than 1 Hz with low-level autonomous reflex controllers running upwards of 300 Hz. We characterize the reflex system by comparing the volume of the set of successful grasps for a naive baseline controller and variations of our reflexive grasping controller, finding that our controller expands the set of successful grasps by 55% relative to the baseline. We also deploy our reflexive grasping controller with a simple vision-based planner in an autonomous clutter clearing task, achieving a grasp success rate above 90% while clearing over 100 items.

## I. INTRODUCTION

Achieving human-like versatility in robotic manipulation will depend on developing hands that are as nimble and reactive as human hands. Much work has been done on developing taxonomies and design requirements for hands [1], [2]. Still, state-of-the-art manipulation systems have not yet been able to replicate the human hand’s functionality.

Instead, many modern approaches rely on hardware initially intended for slow and precise tasks and deploy learning algorithms that depend on large amounts of vision data to carefully plan grasps [3]–[5]. These algorithms can plan the entire manipulation process, from arm motion down to fingertip contacts, but the high latency introduced by the vision systems results in grasping controllers that are unable to react while interacting with objects, which requires high control bandwidth. Even if the planning algorithms use contact and force data, the bandwidth of the vision system limits the execution speed and usually requires that the manipulation plan is quasi-static.

We summarize the challenges faced by robotic manipulation systems as the “last centimeter problem”, inspired by the “last mile problem” for delivery of goods. In our “last centimeter problem”, the unpredictability of contact with neighboring objects and the environment during the final stages of a grasp attempt and the risk of excessively

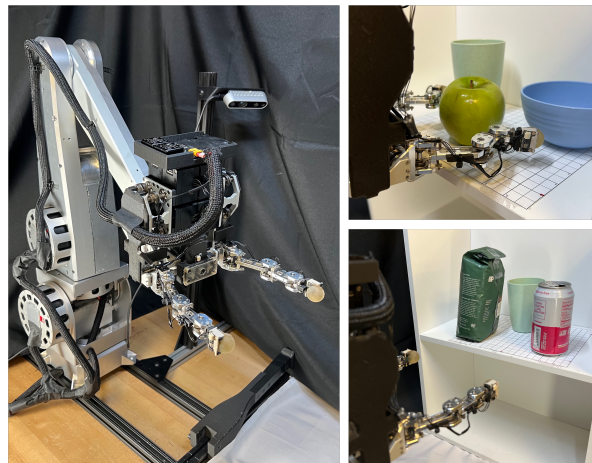


Fig. 1. **Manipulation platform with reflexes for autonomous grasping.** Our reflexive grasping controllers utilize our manipulation platform’s high-bandwidth actuation and low-latency sensing modalities to perform autonomous grasping tasks, such as clearing a cluttered shelf.

disturbing the object to be grasped can impose harsh constraints on the entire manipulation plan, resulting in slow or conservative actions. The dependence of many robotic manipulation systems on vision data exacerbates this challenge, as the cameras that record manipulation scenes often become occluded during the final stages of manipulation plans.

We propose a holistic method of designing manipulation systems while considering both hardware and controller requirements, starting from low-level, high-bandwidth behaviors, which we call reflexes. For fast and robust manipulation, precise trajectory planning is insufficient: the real world is too messy and noisy and inevitably requires repetitive planning. However, we find that given enough high-bandwidth robustness, precise planning is also not necessary: to achieve this robustness, we deliberately avoid carefully integrated high- and low-level plans. We focus instead on increasing the control bandwidth of a low-level, reflexive controller that is fully decoupled from a simple and imprecise high-level planner. These reflexes layer in robustness and resilience through redundancy and are reminiscent of the subsumption architecture pioneered by Brooks [6]. As reflexes are constructed to reason about contact interactions, finger motions, and potentially arm motions, the scope of a higher-level planner is reduced to reasoning only about the manipulation task. In our current system, we use these reflexes to close the grasping feedback loop locally in the hand without needing vision data or adding unnecessary planning complexity. Fig. 2 compares traditional manipulation system architectures with our proposed system.

<sup>1</sup>Authors are with the Biomimetic Robotics Laboratory at the Department of Mechanical Engineering, Massachusetts Institute of Technology (MIT), Cambridge, MA, 02139, USA. saloutos@mit.edu

This work was supported by the Advanced Robotics Lab of LG Electronics Co., Ltd. and the Toyota Research Institute (TRI).

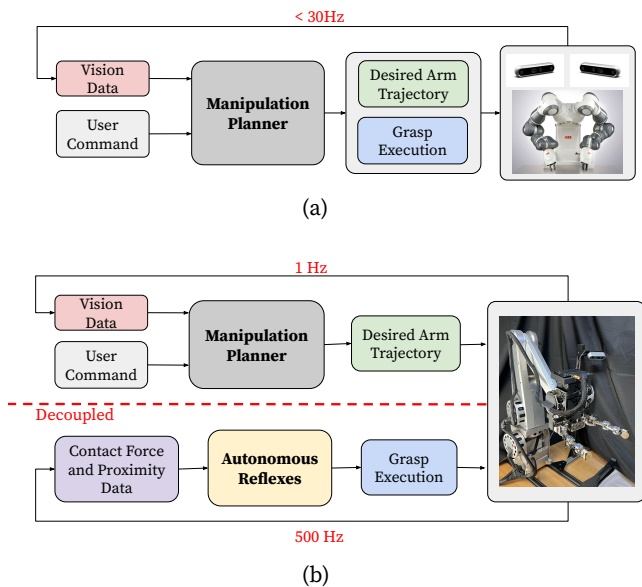


Fig. 2. **Manipulation control architectures.** Traditional, monolithic control architectures (a) are bottle-necked by the sampling frequency of the slowest sensor. Despite efforts to speed up frame rates and signal processing, bandwidths of vision-based control loops are typically limited to below 30 Hz. Our proposed control architecture (b) is decoupled into a slow, high-level planner and a layer of fast, autonomous reflexes that do not depend on vision data to achieve high control bandwidths of 500 Hz.

We introduce a reflexive manipulation algorithm for autonomous grasping and deploy it on our manipulation platform, which has high actuation bandwidth, dexterous fingers, and low-latency multimodal tactile sensors [7]. To demonstrate the performance of the reflexes, we present two experiments. Our first experiment compares our reflexive grasping controller to a naive baseline grasp controller on a pick-and-place task. In our second experiment, we integrate our controller with a simple vision-based planner to complete an autonomous clutter-clearing task.

## II. RELATED WORK

Manipulation performance depends on the robot hardware and the control and planning systems. Our hardware is uniquely high-bandwidth, enabling faster performance than typical systems. Our reflex-based grasping controller replaces low-level primitives, which can be simple routines or more complex reactive controllers, and integrates with other planning algorithms, like those used in end-to-end grasping pipelines.

### A. Hardware for Manipulation

Hardware platforms developed for grasping and manipulation are typically designed to be precise above all else and are best suited for the factory floor. These systems combine stiff, high-inertia arms with end-effectors that are non-backdrivable and have limited force control capabilities, resulting in severely reduced dynamic capabilities. Typical off-the-shelf robot arms, such as the UR5 or Kuka iiwa, have high gear ratios and are not backdrivable. Instead, torque sensors are needed at each joint to close the force control

loop, which limits the bandwidth and makes the systems stiff to collisions. To achieve reflexive manipulation at human-level performance, we developed a fast proprioceptive manipulation platform [7] based on the design principles developed for the Mini Cheetah [8]. The LIMS platform [9] achieves similar design goals; however, it uses a cable-driven design which significantly increases complexity.

Tactile sensing plays a vital role in the abilities of manipulation systems. Recently, the most common tactile sensors used have been vision-based systems such as Gelsight, Digit and the Soft-Bubble grippers [10]–[12]. These offer large amounts of data and are well suited to integration into learning pipelines. However, they suffer from high latency, and a large amount of computation power is necessary to process the video stream. Traditional force-torque sensors offer low latency and high accuracy sensing but are too large for manipulation systems and suffer from acceleration-induced noise. We have presented a multimodal tactile sensor with low-latency force, contact location and proximity data [13], which we will use in this paper to enable our reflexive grasping controllers.

Parallel-jaw grippers are the most common topology used in manipulation research [14], [15], including common off-the-shelf designs such as the Robotiq 2F-85 gripper [16]. These are simple to integrate; however, they are often not backdrivable and have limited or low-bandwidth force control. Robotic hands with more degrees of freedom include the Shadow hand [17], Allegro hand [18], and the DLR hand [19]. Although these offer a wider range of capabilities, they suffer from similar issues: they have low force control bandwidths, little ability to handle collisions, and are fragile.

More recently, Lin *et al.* [20] and Bhatia *et al.* [21] have studied reducing reflected inertia for impact-capable manipulation. These design philosophies are critical for manipulation systems to operate in the real world, where they will face unexpected collisions and changes in the environment. The hardware platform we present in this paper uses similar design principles applied to a higher degree-of-freedom system.

### B. End-to-end Software Pipelines for Grasping

The most common structure for recent manipulation systems has been an end-to-end system focusing on planning with vision data from both traditional cameras and vision-based tactile sensors. These pipelines are generally built with supervised learning or RL algorithms [22]. These systems are capable of a wide range of manipulation tasks [4] [15]. However, they face some bottlenecks when moving from the research lab to the real world. They plan trajectories that are often executed open-loop [14], which means they cannot adjust to environmental changes. Even in systems that use closed-loop control, the low-bandwidth nature of the vision data feedback combined with the high processing times needed to parse this data leads to end-to-end control bandwidths typically ranging from 5-50 Hz [23]–[25]. The bandwidth of the dynamics of the environments that these platforms interact with, small and relatively lightweight

objects, can be orders of magnitude higher than this, making it challenging to respond in real-time to unforeseen changes in the environment. This mismatch in dynamic bandwidth leads to systems operating quasi-statically to avoid disturbing the environment and taking as long as 20 to 60 seconds to complete a single grasp, which is significantly slower than a human. To avoid this, we propose a new structure built from fast and reactive reflexes, compared to traditional planning systems in Fig. 2.

### C. Reactive Grasping Controllers

Reactive grasping controllers have been explored previously, using both tactile and proximity data to make quick adjustments to the system [26], [27]. The most common reaction during grasping is slip control, which typically uses a tactile sensor to determine when the object is slipping out of the hand [28], [29].

Other work has shown reactions based on local analog proximity signals to guide the hand around the object to ensure an enveloped grasp [30].

In our prior work, we developed a slip detection reflex and an antipodal re-grasping reflex with a single degree-of-freedom gripper [7] which enabled higher speed and robustness during teleoperated manipulation. For these types of reflexes to work effectively, they require low-latency sensing and high-bandwidth force control at the gripper. In this work, we present several reflex designs in an integrated system that can handle various disturbances and scenarios.

## III. MANIPULATION PLATFORM

Our manipulation system is shown in the left of Fig. 1. It consists of a low-inertia, high-speed arm and a dexterous two-finger gripper. Each fingertip has a multimodal contact and proximity sensor.

The arm has seven degrees of freedom: three at the shoulder, one at the elbow, and three at the wrist. The three wrist joint axes intersect at the same point, creating a spherical joint. To include the seventh degree of freedom at the wrist, we added a Dynamixel XM540 actuator to the wrist of the design presented in our previous work [7]. The additional degree of redundancy in the wrist pose is important for autonomous grasping as it allows for optimization of arm configurations given planned grasp locations or poses, as opposed to having at most one inverse kinematics solution for the desired grasp pose.

The gripper has two cable-driven fingers, each with four degrees of freedom. Fig. 3 shows the fingers with labeled joint axes. Each finger joint is driven by an antagonistic pair of tungsten cables routed through the finger to Dynamixel XM430 actuators. All actuators are packed as close as possible to the axes of the wrist to minimize inertia while maintaining a wide range of motion. The finger linkages are made of 7075-T6 aluminum alloy, with ball bearings supporting every joint shaft and routing pulley. It is lightweight and low-friction, enabling nimble manipulation actions. The total gripper mass, including the wrist roll actuator, is approximately 1.2 kg. We use a custom PCB for the gripper to

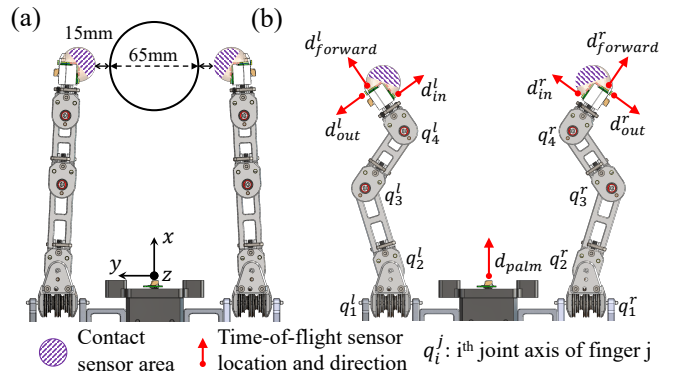


Fig. 3. **Dexterous gripper with multimodal sensors.** Our system uses a two-fingered gripper with multimodal fingertip sensors. The contact sensor areas, time-of-flight proximity sensor directions, and joint axes are also labeled. (a) The nominal pose for the baseline grasping controller in Sec. V-A. The finger width is set based on the cup diameter plus a clearance threshold. (b) The nominal pose for the reflex controllers in Sec. V-A.

receive CAN commands from the control computer, perform current control for the Dynamixel actuators, and send back gripper states and sensor information to the control computer.

Each joint in the arm and fingers, represented by  $q^i$ , is torque-controlled using a PD controller with a feedforward torque term:

$$\tau_{command}^i = K_p^i(q_{des}^i - q^i) + K_d^i(\dot{q}_{des}^i - \dot{q}^i) + \tau_{ff}^i \quad (1)$$

The control computer updates the desired positions, desired velocities, and torque commands at roughly 300 Hz. The controllers for the arm actuators run at 1 kHz, and the controllers for the Dynamixels run at 500 Hz.

Each fingertip has a multimodal sensor that can return contact force, location, and proximity data [13], shown in Fig. 3. The sensor measures the 2-D contact location over its spherical surface, parameterized by the angles  $\theta$  and  $\phi$ , and estimates the 3-D contact force at that location,  $F = [f_x, f_y, f_z]$ . The z-component of the contact force is the contact normal force, and the x- and y-components are the contact shear forces. In addition to the contact data, the fingertip sensors capture pre-touch information from proximity data along three outward directions. We also use a proximity sensor in the palm, and the vector of proximity data is given by:

$$d = [d_{out}^l, d_{forward}^l, d_{in}^l, d_{palm}, d_{in}^r, d_{forward}^r, d_{out}^r] \quad (2)$$

The individual sensors are sampled at 200 Hz, with minimal time for processing overhead.

## IV. REFLEXIVE GRASPING ALGORITHM

Fig. 4 shows a flowchart detailing our reflexive grasping controller. The only high-level plan necessary for our reflexive grasping controller is the current location of an object to be grasped and the desired final location for it. Once the controller receives a target grasping location, the arm moves the gripper towards the target, activating individual reflexes or combinations of reflexes along the way. The reflexes use the arm and finger kinematics, force and proximity data, and contact kinematics to perform fast and robust grasping below the planning level.

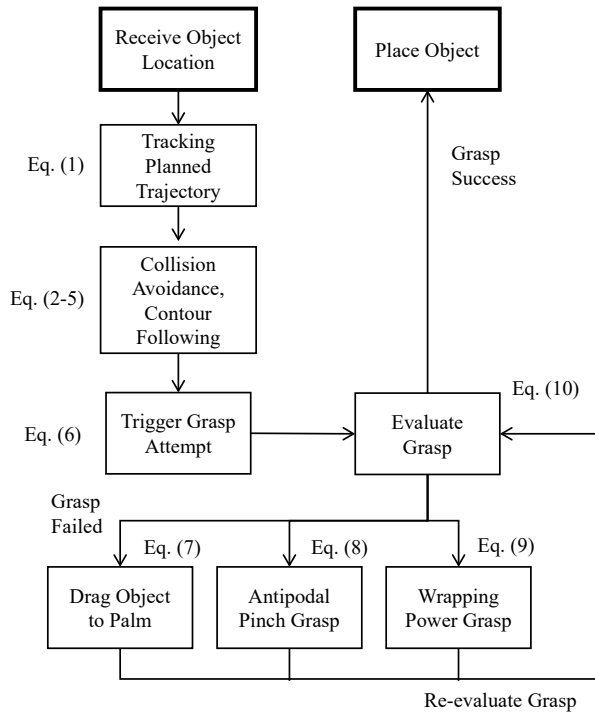


Fig. 4. **Behaviour tree for reflexive grasping.** As the arm moves the gripper to the target location, the autonomous reflexes attempt to grasp the object. The high-level planner only needs to provide the target object location to the controller.

#### A. Collision Avoidance and Contour Following

As the hand approaches the target grasping location, the fingers hold a nominal “open hand” pose, shown in Fig. 3. The data from the proximity sensors are used to create virtual potential fields around the fingertips, with different stiffnesses and activation distances for each sensing direction from the fingertip: outwards, forwards, and inwards. The sum of the forces from the individual potential fields yields a net force on the fingertip, given by:

$$\mathbf{F}^i = \alpha_{out} K_{out} (d_{out} - d_{out}^{des}) \mathbf{e}_{out} + \alpha_{forward} K_{forward} (d_{forward} - d_{forward}^{des}) \mathbf{e}_{forward} + \alpha_{in} K_{in} (d_{in} - d_{in}^{des}) \mathbf{e}_{in} \quad (3)$$

where each  $\alpha_i$  is an activation coefficient, each  $\mathbf{e}_i$  is a unit vector along the corresponding direction from the fingertip, and stiffnesses and measured distances are represented by  $K_i$  and  $d_i$ , respectively. The coefficients  $\alpha_i$  are determined by the threshold conditions:

$$\alpha_{out} = (d_{out} < d_{out}^{thresh}) \\ \alpha_{forward} = (d_{forward} < d_{forward}^{thresh}) \\ \alpha_{in} = (d_{in} < d_{in}^{thresh}) \quad (4)$$

The virtual potential fields due to the outward and forward proximity sensors are activated as soon as the measured distance goes below a threshold, so they are only repulsive. The nominal distance for the potential fields,  $d^{des}$ , is the same as the activation threshold,  $d^{thresh}$ . For these two directions, the forces on the fingertips enable reactive collision and obstacle avoidance. The potential fields due to the inward

TABLE I  
ALGORITHM PARAMETERS

Purpose	Symbol	Value
Potential field distances	$(d_{out}^{thresh}, d_{forward}^{thresh}, d_{in}^{thresh}, d_{in}^{des})$	(9, 9, 9, 6) cm
Potential field stiffnesses	$(K_{out}, K_{forward}, K_{in})$	(20, 30, 12) $\frac{N}{m}$
Grasp triggering thresholds	$(d_{near}, d_{far}, d_{occlude})$	(0.05, 0.09, 0.04) cm
Antipodal angle threshold	$\gamma_a$	20°
Re-grasping radius threshold	$r_{power}$	3 cm
Grasp success thresholds	$(\gamma_s, \gamma_f)$	(0.2 $\frac{m}{s}$ , 0.5 N)
Grasp termination time	$t_{fail}$	3.0 s

proximity sensors can be attractive and repulsive, as the activation threshold is not the nominal distance. Once an object is within the activation threshold, the fingertip will attempt to maintain the desired distance from the object’s surface, which yields a contour following behavior that allows the fingertips to react to object shapes and to passively wrap around objects while the hand is advancing to the target grasp position.

$$d_{out}^{des} = d_{out}^{thresh} \\ d_{forward}^{des} = d_{forward}^{thresh} \\ d_{in}^{des} < d_{in}^{thresh} \quad (5)$$

#### B. Triggering and Evaluating Grasp Attempts

While the hand is moving towards the target grasp location, several conditions can trigger an early grasp attempt based on the proximity data and finger kinematics. These conditions are represented by  $\beta_i$ :

$$\beta_{near} = (d_{palm} < d_{near}) \\ \beta_{far} = (d_{palm} < d_{far}) \\ \beta_{tips} = (q_{iip}^l < \theta_{close}) \wedge (q_{iip}^r < \theta_{close}) \\ \beta_{occlude} = (d_{forward}^l < d_{occlude}) \vee (d_{forward}^r < d_{occlude}) \quad (6)$$

where  $q_{iip}^l$  and  $q_{iip}^r$  are the fingertip angles in the gripper frame. The conditions  $\beta_{near}$  and  $\beta_{far}$  are based primarily on the palm proximity measurement and indicate that the object is between the fingers and close enough to the palm to be grasped. With the condition  $\beta_{tips}$ , a grasp can be triggered if the fingertips have wrapped around the object. Finally, for  $\beta_{occlude}$ , if the forward proximity measurement is too low, the finger is occluded and cannot proceed with the grasp. Since the controller can initiate a re-grasping attempt, it can rely on the re-grasping if a finger is blocked rather than causing the grasp attempt to fail. If the gripper reaches the final grasp target without a grasp already being triggered, a grasp attempt is initiated anyways.

#### C. Re-grasping Decisions

Once a grasp has been attempted, the controller evaluates contact forces and kinematics to determine if the grasp was successful or if a re-grasp needs to be attempted. Using the measured contact frames, the controller approximates the object as a circle and estimates the radius and location in the gripper frame,  $r_{obj}$  and  $(x_{obj}, y_{obj}, z_{obj})$ . Based on the differences between the x-coordinates of the fingertip



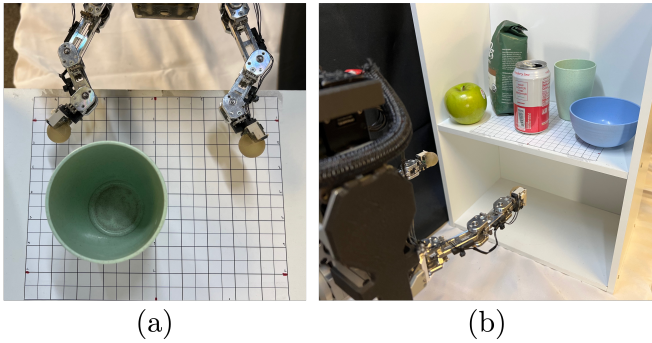


Fig. 5. **Experimental setups.** (a) The 12.5 mm grid and sample cup used to characterize the reflexive grasping controllers. (b) The variety of kitchen objects used for the autonomous clutter-clearing experiment.

locations in the gripper frame,  $x_{tip}^l$  and  $x_{tip}^r$ , and the x-coordinate of the object location,  $x_{obj}$ , the controller plans one of three re-grasps:

- If  $x_{obj} > x_{tip}^l$  and  $x_{obj} > x_{tip}^r$ , the re-grasping trajectory pinches the object and pulls it closer to the palm. Then, the fingers are moved forward to achieve an antipodal pinch grasp, based on the new object location and the estimated radius,  $r_{obj}$ . (7)
- If  $x_{obj} < x_{tip}^l$  and  $x_{obj} < x_{tip}^r$ , the fingertips have successfully wrapped around the object, but the grasp has not been declared successful. If the object radius is less than a threshold,  $r_{obj} < r_{power}$ , the controller plans an antipodal pinch grasp by moving the fingertips back towards the palm. (8)
- Otherwise, the controller plans to extend the fingers to wrap around the object into a more secure power grasp. If the signs of the differences between the fingertip x-coordinates and the object x-coordinate do not match, the controller also plans a wrapping power grasp. (9)

After the re-grasping trajectory is completed, the resulting grasp is evaluated again.

#### D. Evaluating Grasp Attempts

Grasp attempts are evaluated using information from fingertip and palm proximity measurements, contact forces, and contact kinematics. The controller declares a successful grasp when both fingertips have stopped moving, both contact normal forces are above a threshold, and the object is seen by the palm proximity sensor, represented as:

$$\beta_{success} = (v_{tip}^l < \gamma_v) \wedge (v_{tip}^r < \gamma_v) \wedge (|F_z^l| > \gamma_F) \wedge (|F_z^r| > \gamma_F) \wedge \beta_{far} \quad (10)$$

After a grasp has been triggered, the controller will attempt to grasp for a set amount of time before declaring failure,  $t_{fail}$ .

## V. EXPERIMENTS

We present two grasping experiments using our reflexive grasping system. In the first experiment, we characterize the difference in grasping capabilities between variations of our reflexive controller and a naive baseline controller. In the second experiment, we use the reflexes to achieve robust autonomous grasping for a clutter-clearing task.

### A. Reflex Characterization

For this experiment, we command the robot to repeatedly perform a pick-and-place task from a constant location, called the nominal grasp location. To characterize the robustness of the grasping controllers, we record the set of successful grasps as the object is moved further and further from the nominal grasp location along a 12.5 mm grid. Displacing the object without changing the commanded grasp location isolates the effectiveness of the controllers from the measurement noise inherent to vision-based systems. For a successful grasp, the gripper must grasp the object and then transport it to a predetermined “place” position. Fig. 5a shows the experiment setup with the fixed grid and the sample object, a cup that is roughly 110 mm tall and 65 mm in diameter.

We characterize the performance of three grasping controllers. The first controller is a naive baseline that performs a simple closing maneuver without any feedback information from the fingers or the fingertip sensors. The distance between the fingertips is chosen to be slightly wider than the cup diameter, as if the grasp command included the desired location and gripper width [23].

The second controller, called the partial-reflex controller, uses the collision avoidance and contour following reflexes but does not use the re-grasping reflex. The third controller uses all of the reflexes, including re-grasping, so it is called the full-reflex controller. For these controllers, the fingertips are spread wider apart to improve the effectiveness of the contour following. The collision avoidance reflex mitigates any collisions that could happen during grasping with undesired objects or the environment due to the wider pose.

Fig. 6 shows the set of successful grasps for each of the three controllers. The contour following in the partial-reflex controller increases the width of the set near the nominal grasp location. The re-grasping capabilities of the full-reflex controller are necessary to expand the set of successful grasps further away from the nominal location. Based on the area covered by each controller, the set of successful grasps for the partial-reflex controller is 29.2% larger than the set for the baseline controller. The full-reflex controller achieves a 20.4% increase relative to the partial-reflex controller and a 55.6% increase relative to the baseline controller. Each increase in the volumes of the sets of successful grasps can be interpreted as an increase in overall grasp robustness due to the additional reflex-based controllers since the input to each controller is constant.

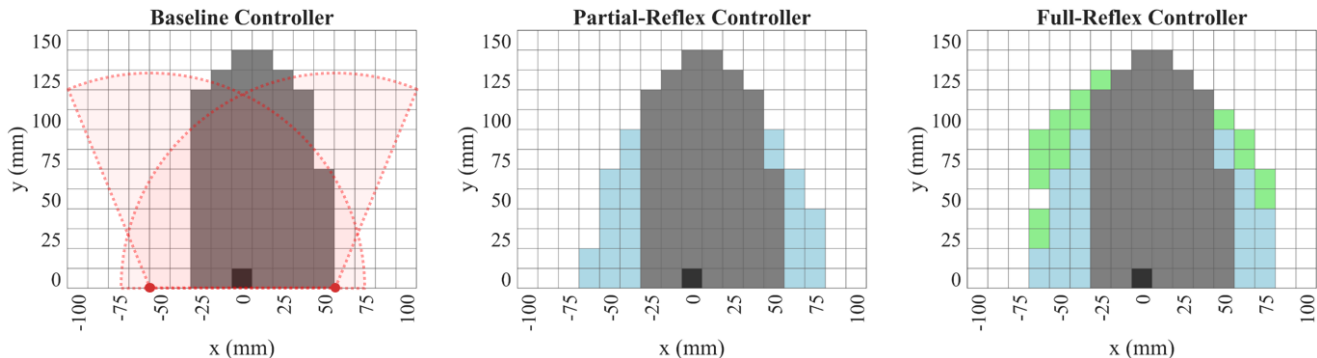


Fig. 6. **Characterizing the reflexive grasping controller.** As reflexes are added to the baseline grasp controller, the set of successful grasps expands. On the left-most plot, the base of each finger is marked by a red dot and the workspace is shown in red. The set of successful grasps for the baseline controller is shown in light grey on each grid plot, and the nominal grasp location is shown in dark grey. The expanded set of grid locations covered by the partial-reflex controller is shown in light blue, and the further expanded set of grid locations covered by the full-reflex controller is shown in green. The set of successful grasps for the baseline controller covers 11250 mm<sup>2</sup>. The total areas for the partial-reflex and full-reflex controllers are 14530 mm<sup>2</sup> and 17500 mm<sup>2</sup>, respectively.

### B. Autonomous Grasping for Clutter-Clearing

For this experiment, we combine our reflexive grasping controller with a vision algorithm for object identification to autonomously grasp objects from a cluttered shelf. An Intel Realsense D435i camera is used to capture an image of the cluttered shelf, and the YOLOv7 [31] object classifier is used to detect graspable objects within the RGB image. A point cloud is extracted from the depth image for the closest identified object. Outlier points, defined by the top and bottom 10% of depth measurements, are removed from the object point cloud, and the mean  $(x, y, z)$  location of the remaining points in the world frame is sent as the target grasping location. During grasping, the desired wrist pose is set so that the gripper stays in the horizontal plane and that the inverse kinematics for the rest of the arm joint angles can be quickly solved analytically. After startup, the only human involvement in the system is placing more objects into the environment. The objects used include an apple, a bowl, a can, a bag of coffee grounds, and a cup, and they are shown in Fig. 5b.

Table II shows the grasping success rates for each object. Across 117 total attempted grasps, the success rate is 90.6%. While the bowl has by far the lowest grasp success rate at 68%, the other objects have an average grasp success rate of 94%. Across all successful grasps, the average time per grasp was 7.1 seconds. This time included an average of 4.5 seconds for picking the objects, including the approach trajectory, and an average of 2.6 seconds for placing the objects. For context, the objects were placed approximately 35 cm away from the start of the grasping trajectory, which is within one human arm-length.

## VI. DISCUSSION AND CONCLUSION

Our experiments demonstrate improved robustness at three levels. First, the reflexes improve grasping robustness to environmental uncertainties, such as noisy or occluded vision data, unstable objects, or unusual object shapes. Second, the reflexes improve robustness to trajectory plans, allowing for simpler and slower planning, either from a high-level planner

TABLE II  
GRASPING SUCCESS RATES

Object	Trials	Successes	Success Rate
Apple	26	25	96%
Coffee	25	24	96%
Cup	26	24	92%
Can	24	22	92%
Bowl	16	11	68%
<b>Total</b>	<b>117</b>	<b>106</b>	<b>90.6%</b>

or an operator. This feature allows the planner to focus on high-level tasks instead of providing precise visual servoing. Finally, our system achieves high-speed manipulation at a human scale with minimal impulses and collisions, which is critical for safe interaction that does not damage the environment or the robot.

Our current set of reflexes has been designed ad-hoc for everyday household objects, which fit very well into a relatively limited range of sizes and shapes. In future work, we aim to expand the range of reflexes to account for broader classes of objects with different properties. We believe that building toward general manipulation capability, reliability, and flexibility will require layering many decoupled reflexes to address different scenarios in parallel instead of deploying a single do-it-all controller. It may be possible, nonetheless, to generalize a design or develop a learning paradigm to automatically synthesize new reflexes as new scenarios are encountered.

We have shown a reflexive grasping algorithm that allows for robust autonomous grasping, even with a simple grasp planning algorithm. The reflexes are designed to exploit our low-inertia manipulation platform and high-bandwidth sensors, and by decoupling the reflexive control from manipulation planning, the planner is able to operate at a much lower frequency than the reflex controllers: it is not responsible for solving the “last centimeter” problem.

## ACKNOWLEDGMENTS

The authors would like to thank Steve Heim for his thoughtful discussions and feedback.

## REFERENCES

- [1] I. M. Bullock, R. R. Ma, and A. M. Dollar, "A hand-centric classification of human and robot dexterous manipulation," *IEEE transactions on Haptics*, vol. 6, no. 2, pp. 129–144, 2012.
- [2] T. Feix, J. Romero, H.-B. Schmedtmayer, A. M. Dollar, and D. Kragic, "The grasp taxonomy of human grasp types," *IEEE Transactions on human-machine systems*, vol. 46, no. 1, pp. 66–77, 2015.
- [3] N. Fazeli, M. Oller, J. Wu, Z. Wu, J. B. Tenenbaum, and A. Rodriguez, "See, feel, act: Hierarchical learning for complex manipulation skills with multisensory fusion," *Science Robotics*, vol. 4, no. 26, eaav3123, 2019.
- [4] W. Gao and R. Tedrake, "Kpam 2.0: Feedback control for category-level robotic manipulation," *IEEE Robotics and Automation Letters*, vol. 6, no. 2, pp. 2962–2969, 2021.
- [5] A. Zeng, S. Song, K.-T. Yu, E. Donlon, F. R. Hogan, M. Bauza, D. Ma, O. Taylor, M. Liu, E. Romo, *et al.*, "Robotic pick-and-place of novel objects in clutter with multi-affordance grasping and cross-domain image matching," in *2018 IEEE international conference on robotics and automation (ICRA)*, IEEE, 2018, pp. 3750–3757.
- [6] R. Brooks, "A robust layered control system for a mobile robot," *IEEE journal on robotics and automation*, vol. 2, no. 1, pp. 14–23, 1986.
- [7] A. SaLoutos, E. Stanger-Jones, and S. Kim, "Fast reflexive grasping with a proprioceptive teleoperation platform," *arXiv preprint arXiv:2208.04487*, 2022.
- [8] B. Katz, J. Di Carlo, and S. Kim, "Mini cheetah: A platform for pushing the limits of dynamic quadruped control," in *International Conference on Robotics and Automation*, IEEE, 2019, pp. 6295–6301.
- [9] Y.-J. Kim, "Anthropomorphic low-inertia high-stiffness manipulator for high-speed safe interaction," *IEEE Transactions on robotics*, vol. 33, no. 6, pp. 1358–1374, 2017.
- [10] W. Yuan, S. Dong, and E. H. Adelson, "Gelsight: High-resolution robot tactile sensors for estimating geometry and force," *Sensors*, vol. 17, no. 12, p. 2762, 2017.
- [11] N. F. Lepora, Y. Lin, B. Money-Coomes, and J. Lloyd, "Digitac: A digit-tactip hybrid tactile sensor for comparing low-cost high-resolution robot touch," *IEEE Robotics and Automation Letters*, vol. 7, no. 4, pp. 9382–9388, 2022.
- [12] A. Alspach, K. Hashimoto, N. Kuppuswamy, and R. Tedrake, "Soft-bubble: A highly compliant dense geometry tactile sensor for robot manipulation," in *2019 2nd IEEE International Conference on Soft Robotics (RoboSoft)*, IEEE, 2019, pp. 597–604.
- [13] A. SaLoutos, E. Stanger-Jones, M. Guo, H. Kim, and S. Kim, *Design of a multimodal fingertip sensor for dynamic manipulation*, Submitted to ICRA 2023, pre-print is available at: <https://drive.google.com/drive/folders/17irtdNtPQULrBLORc6Bes3trORYMygMF?usp=sharing>.
- [14] A. ten Pas, M. Gualtieri, K. Saenko, and R. Platt, "Grasp pose detection in point clouds," *The International Journal of Robotics Research*, vol. 36, no. 13-14, pp. 1455–1473, 2017.
- [15] S. Dong, D. K. Jha, D. Romeres, S. Kim, D. Nikovski, and A. Rodriguez, "Tactile-rl for insertion: Generalization to objects of unknown geometry," *2021 IEEE International Conference on Robotics and Automation (ICRA)*, 2021.
- [16] *2f-85 and 2f-140 grippers*. [Online]. Available: <https://robotiq.com/products/2f85-140-adaptive-robot-gripper>.
- [17] *Shadow hand*. [Online]. Available: <https://www.shadowrobot.com/dexterous-hand-series/>.
- [18] D.-H. Lee, J.-H. Park, S.-W. Park, M.-H. Baeg, and J.-H. Bae, "Kitech-hand: A highly dexterous and modularized robotic hand," *IEEE/ASME Transactions on Mechatronics*, vol. 22, no. 2, pp. 876–887, 2017.
- [19] J. Butterfaß, M. Grebenstein, H. Liu, and G. Hirzinger, "Dlr-hand ii: Next generation of a dextrous robot hand," in *Proceedings 2001 ICRA. IEEE International Conference on Robotics and Automation (Cat. No. 01CH37164)*, IEEE, vol. 1, 2001, pp. 109–114.
- [20] M. A. Lin, R. Thomasson, G. Uribe, H. Choi, and M. R. Cutkosky, "Exploratory hand: Leveraging safe contact to facilitate manipulation in cluttered spaces," *IEEE Robotics and Automation Letters*, vol. 6, no. 3, pp. 5159–5166, 2021.
- [21] A. Bhatia, A. M. Johnson, and M. T. Mason, "Direct drive hands: Force-motion transparency in gripper design," in *Robotics: science and systems*, 2019.
- [22] D. Kalashnikov, A. Irpan, P. Pastor, J. Ibarz, A. Herzog, E. Jang, D. Quillen, E. Holly, M. Kalakrishnan, V. Vanhoucke, *et al.*, "Scalable deep reinforcement learning for vision-based robotic manipulation," in *Conference on Robot Learning*, PMLR, 2018, pp. 651–673.
- [23] D. Morrison, P. Corke, and J. Leitner, "Closing the loop for robotic grasping: A real-time, generative grasp synthesis approach," *arXiv preprint arXiv:1804.05172*, 2018.
- [24] U. Viereck, A. t. Pas, K. Saenko, and R. Platt, *Learning a visuomotor controller for real world robotic grasping using simulated depth images*, 2017. DOI: 10.48550/ARXIV.1706.04652. [Online]. Available: <https://arxiv.org/abs/1706.04652>.
- [25] D. Morrison, P. Corke, and J. Leitner, "Learning robust, real-time, reactive robotic grasping," *The International Journal of Robotics Research*, vol. 39, no. 2-3, pp. 183–201, 2020. DOI: 10.1177/0278364919859066.
- [26] M. Teichmann and B. Mishra, "Reactive robotics i: Reactive grasping with a modified gripper and multifingered hands," *The International Journal of Robotics Research*, vol. 19, no. 7, pp. 697–708, 2000.
- [27] R. M. Al-Gaifi, V. Müller, and N. Elkmann, "Reactive grasping using high-resolution tactile sensors," in *2020 IEEE 16th International Conference on Automation Science and Engineering (CASE)*, 2020, pp. 463–468.
- [28] D. Gunji, Y. Mizoguchi, S. Teshigawara, A. Ming, A. Namiki, M. Ishikawaand, and M. Shimojo, "Grasping force control of multi-fingered robot hand based on slip detection using tactile sensor," in *2008 IEEE International Conference on Robotics and Automation*, IEEE, 2008, pp. 2605–2610.
- [29] M. Tremblay and M. Cutkosky, "Estimating friction using incipient slip sensing during a manipulation task," in *[1993] Proceedings IEEE International Conference on Robotics and Automation*, 1993, 429–434 vol.1.
- [30] K. Koyama, Y. Suzuki, A. Ming, and M. Shimojo, "Integrated control of a multi-fingered hand and arm using proximity sensors on the fingertips," in *2016 IEEE International Conference on Robotics and Automation (ICRA)*, 2016, pp. 4282–4288.
- [31] C.-Y. Wang, A. Bochkovskiy, and H.-Y. M. Liao, "YOLOv7: Trainable bag-of-freebies sets new state-of-the-art for real-time object detectors," *arXiv preprint arXiv:2207.02696*, 2022.